Electronic Supplementary Material (ESI) for Inorganic Chemistry Frontiers.

Supplementary Information

Anchoring polysulfides via CoS_2/NC@1T MoS_2 modified separator for high-performance lithium-sulfur batteries

Qicheng Li, Hui Liu, Bo Jin,* Lei Li, Qidong Sheng, Mengyang Cui, Yiyang Li, Xingyou Lang, Yongfu Zhu, Lijun Zhao, Qing Jiang*

Key Laboratory of Automobile Materials, Ministry of Education, and School of Materials Science and Engineering, Jilin University, Changchun 130022, China

* Corresponding author. E-mail: jiangq@jlu.edu.cn (Q. Jiang)
* Corresponding author. E-mail: jinbo@jlu.edu.cn (B. Jin)

Supplementary Figures

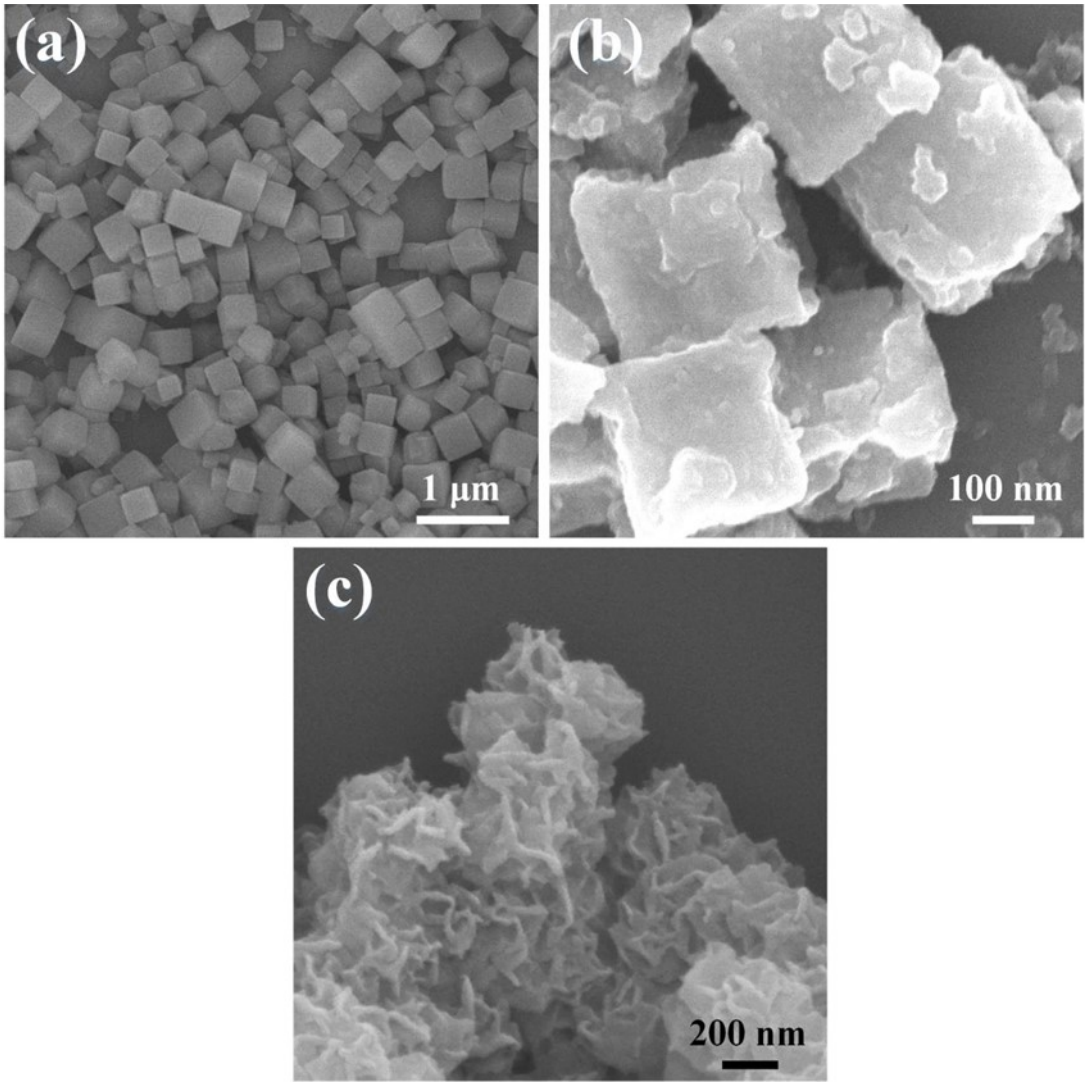

Figure S1 FESEM images of (a) ZIF-67, (b) Co/NC, and (c) CoS_2/NC@1T MoS_2.

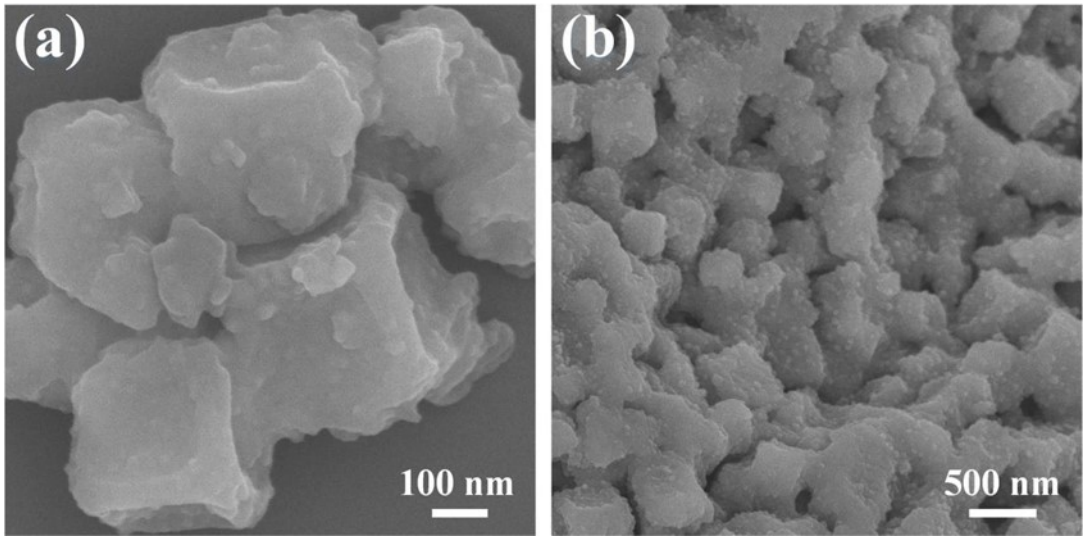

Figure S2 FESEM images of CoS_2/NC with (a) high-resolution and (b) low-resolution.

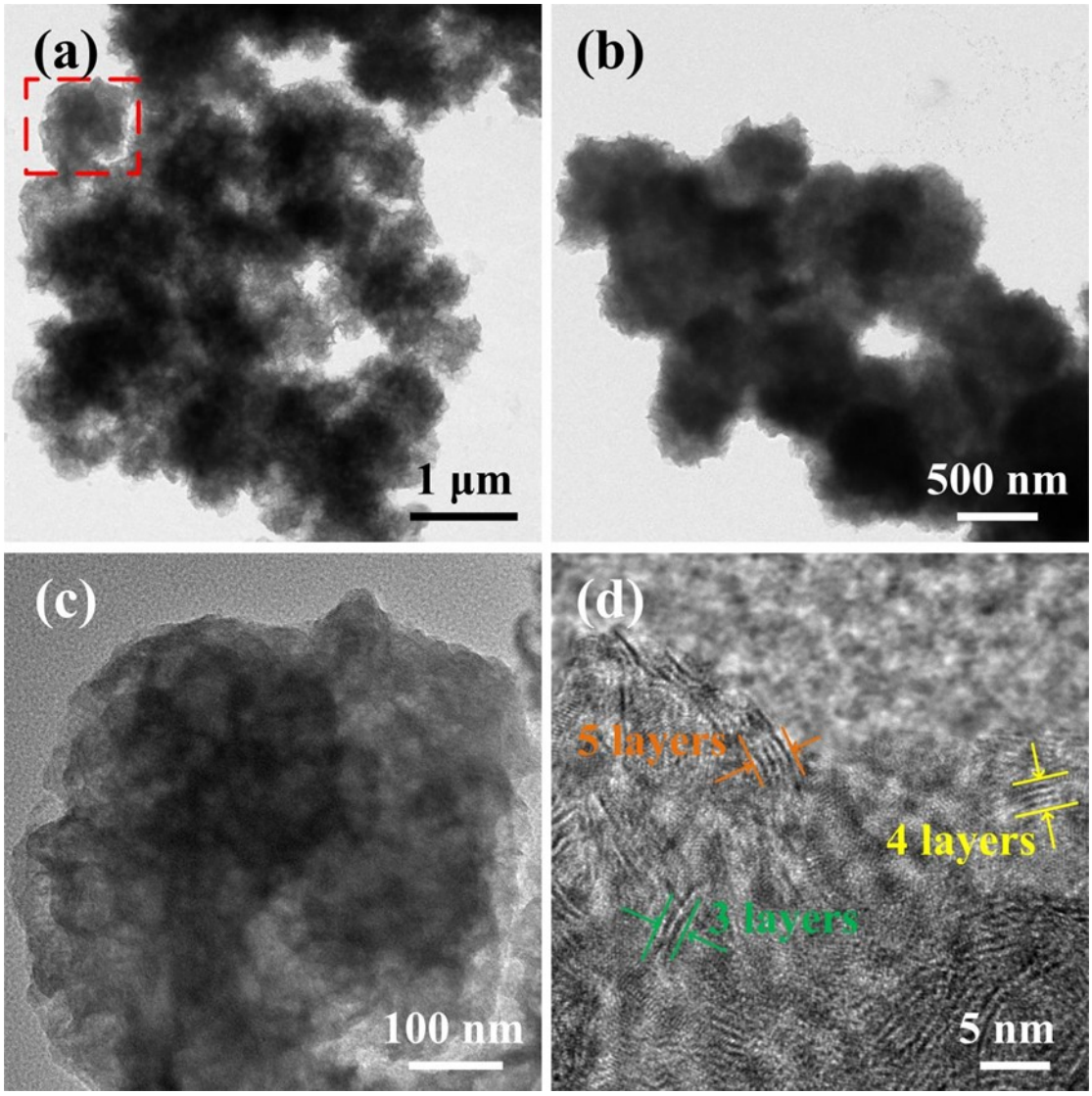

Figure S3 (a,b) TEM images of CoS_2/NC@1T MoS_2 with different magnifications. (c) Enlarged TEM image of the red frame in (a). (d) HRTEM image of CoS_2/NC@1T MoS_2.

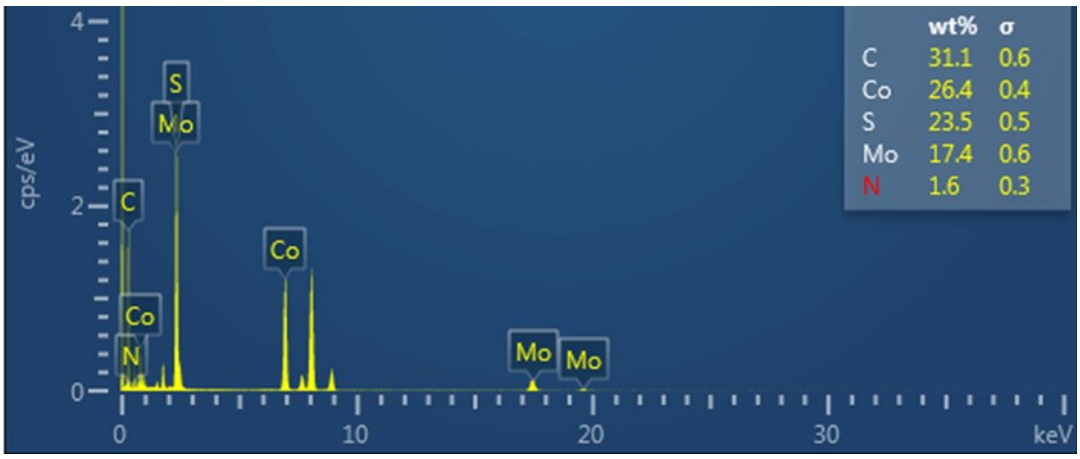

Figure S4 EDS elemental composition diagram of CoS_2/NC@1T MoS_2.

According to the EDS elemental composition diagram of TEM (Figure S4), the total amount of N and C elements in CoS_2/NC@1T MoS_2 is 32.7 wt%. Since Co, Mo, and S elements exist in the form of chemical compounds, we use more accurate inductively coupled plasma emission spectrometry to determine their elemental composition.

To prepare the ICP sample, a certain amount of CoS_2/NC@1T MoS_2 was dissolved in nitric acid, and treated overnight at 60 °C. The as-obtained solution was diluted with deionized water into a concentration of 0.5 mg/L solution. The ICP results show that the concentrations of Mo and Co in CoS_2/NC@1T MoS_2 are 0.0751 and 0.0154 mg/L, respectively. The contents of 1T MoS_2 and CoS_2 are calculated by formulas as follows:

$$1T\ MoS_2$$

$$wt\% = \frac{0.0751\ mg/L \times 160/96}{0.0751\ mg/L \times 160/96 + 0.0154\ mg/L \times 123/59} \times 67.3\% = 53.6\%$$

$$CoS_2\ wt\% = \frac{0.0154\ mg/L \times 123/59}{0.0751\ mg/L \times 160/96 + 0.0154\ mg/L \times 123/59} \times 67.3\% = 13.7\%$$

According to Figure S4 and the above calculations, the contents of each component in CoS_2/NC@1T MoS_2 are 53.6 wt% for 1T MoS_2, 13.7 wt% for CoS_2, and 32.7 wt% for NC, respectively.

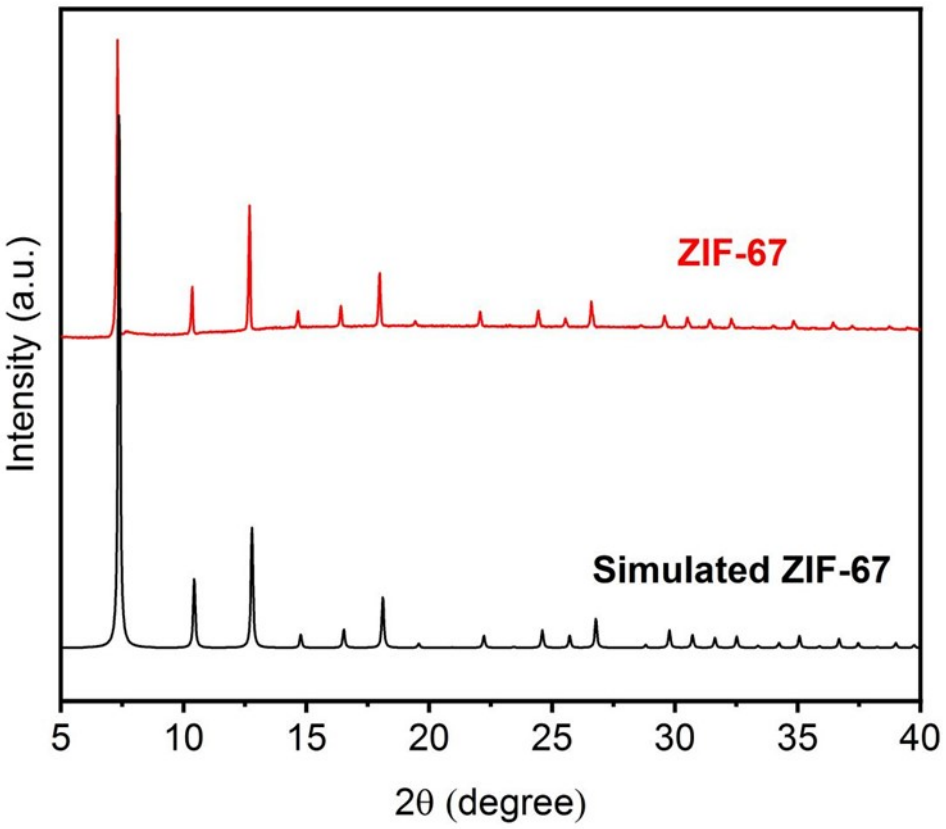

Figure S5 XRD pattern of ZIF-67.

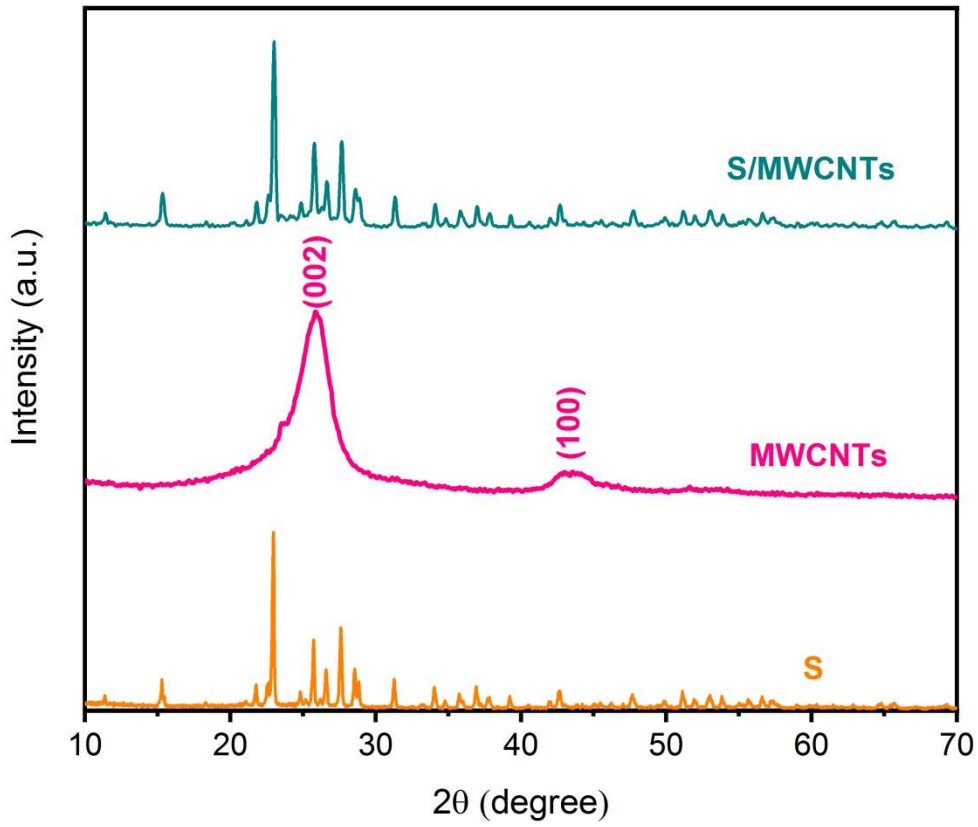

Figure S6 XRD patterns of S, MWCNTs, and S/MWCNTs.

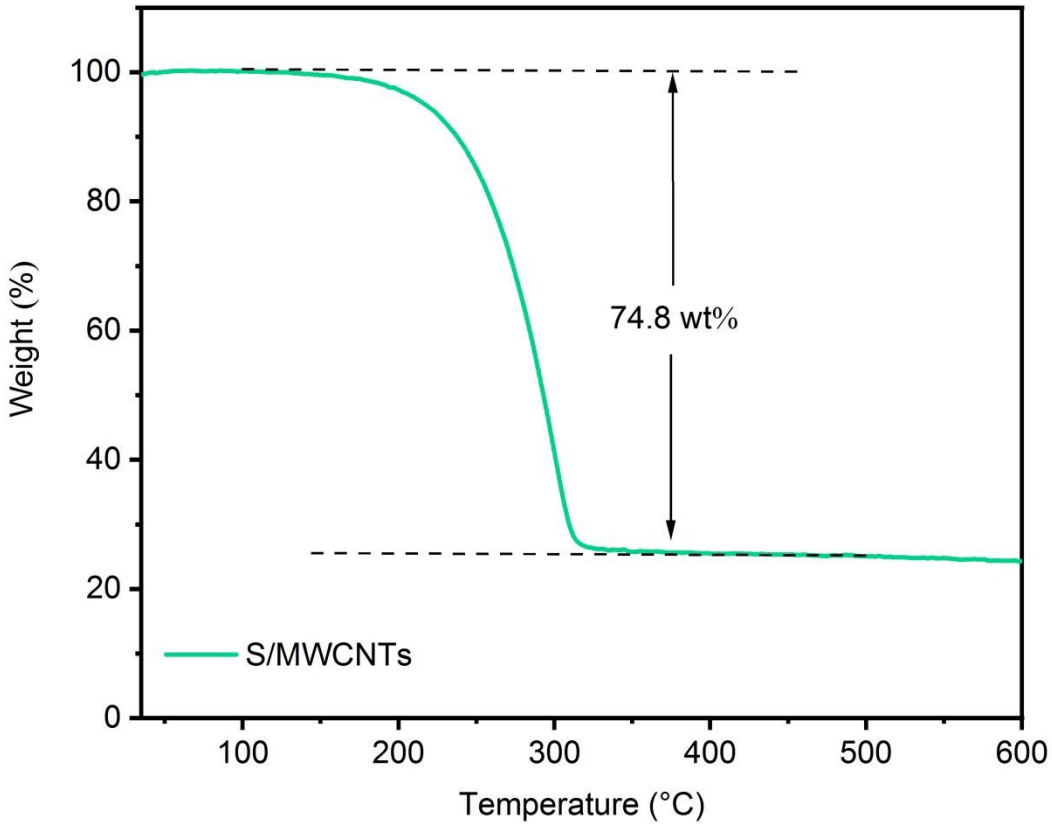

Figure S7 TGA curve of S/MWCNTs.

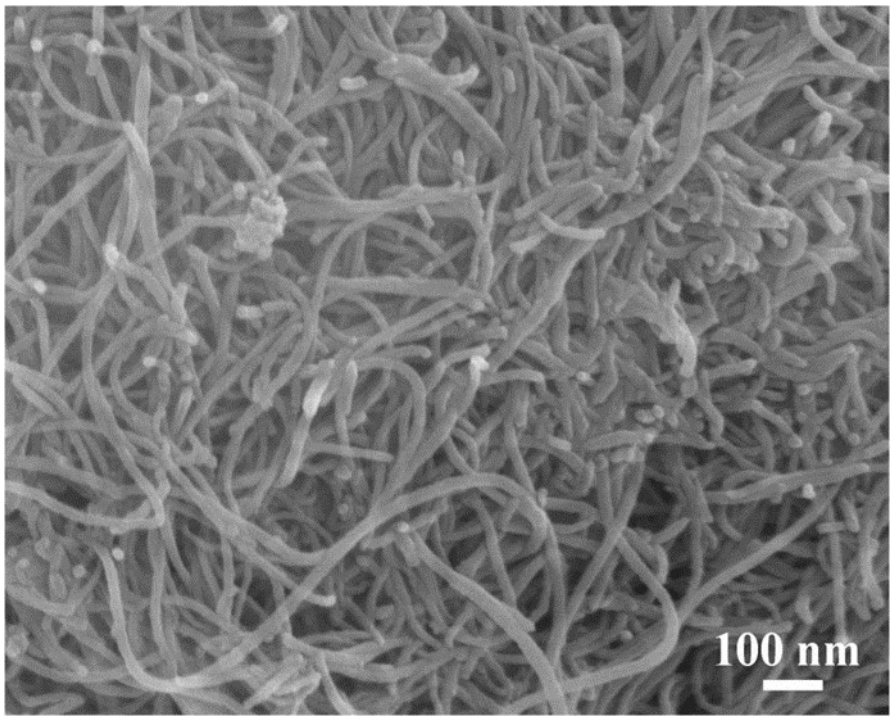

Figure S8 FESEM image of S/MWCNTs.

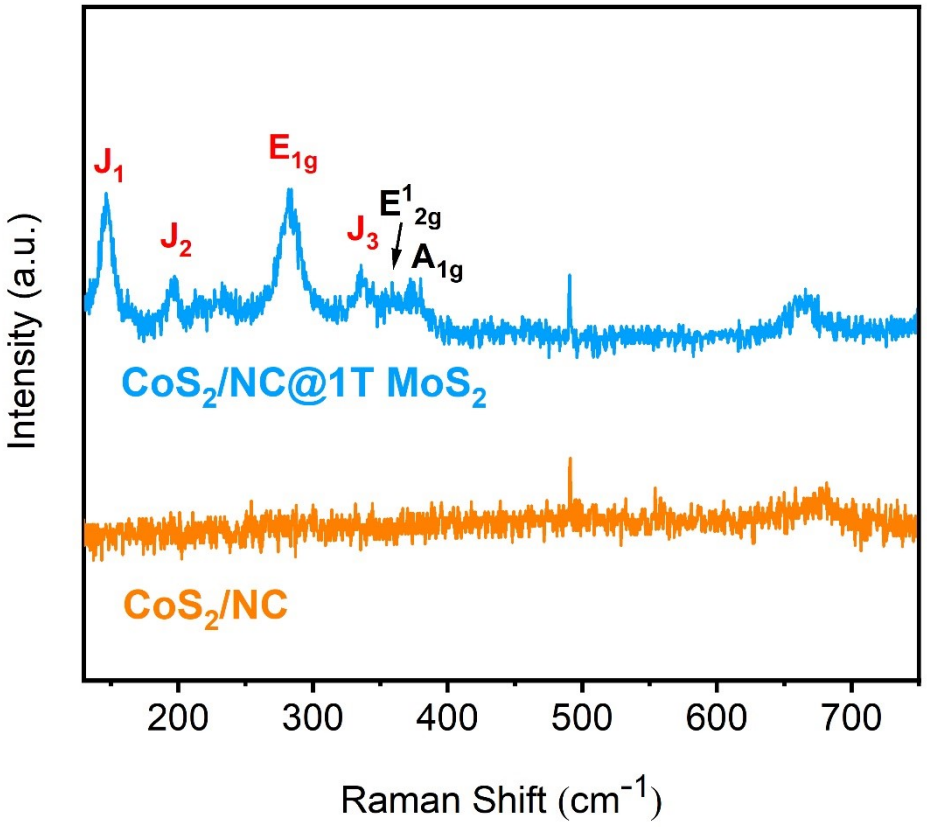

Figure S9 Raman spectra of CoS_2/NC and CoS_2/NC@1T MoS_2 in Raman shift range of 130-750 cm^{-1}.

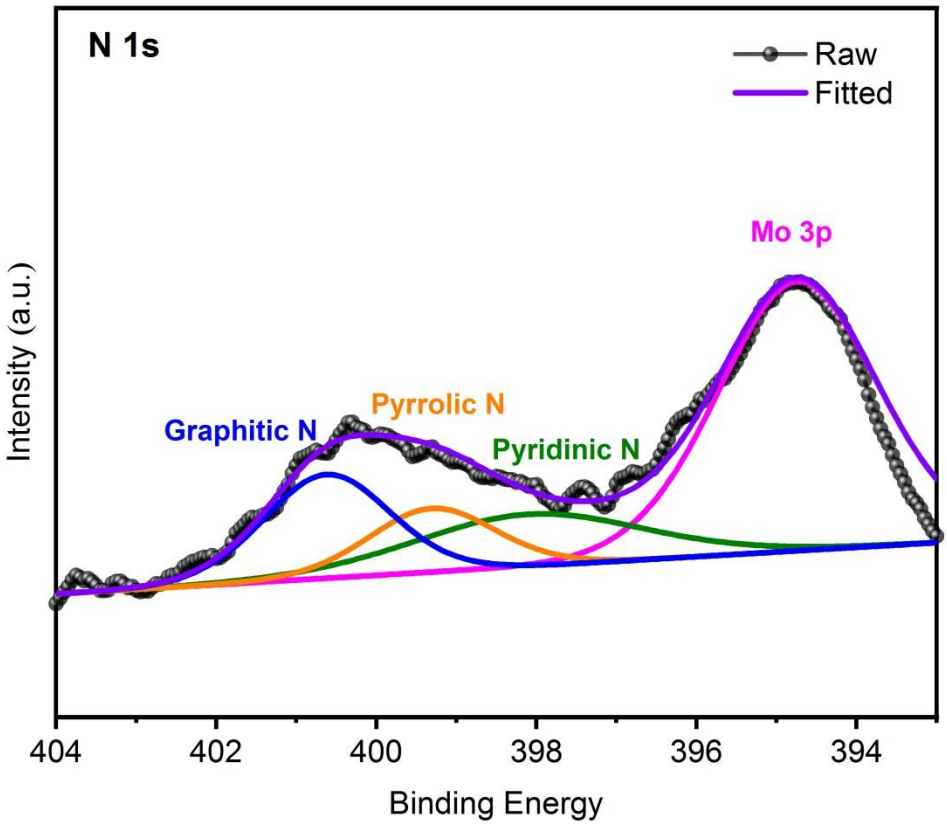

Figure S10 High-resolution XPS spectrum of N 1s of CoS_2/NC@1T MoS_2.

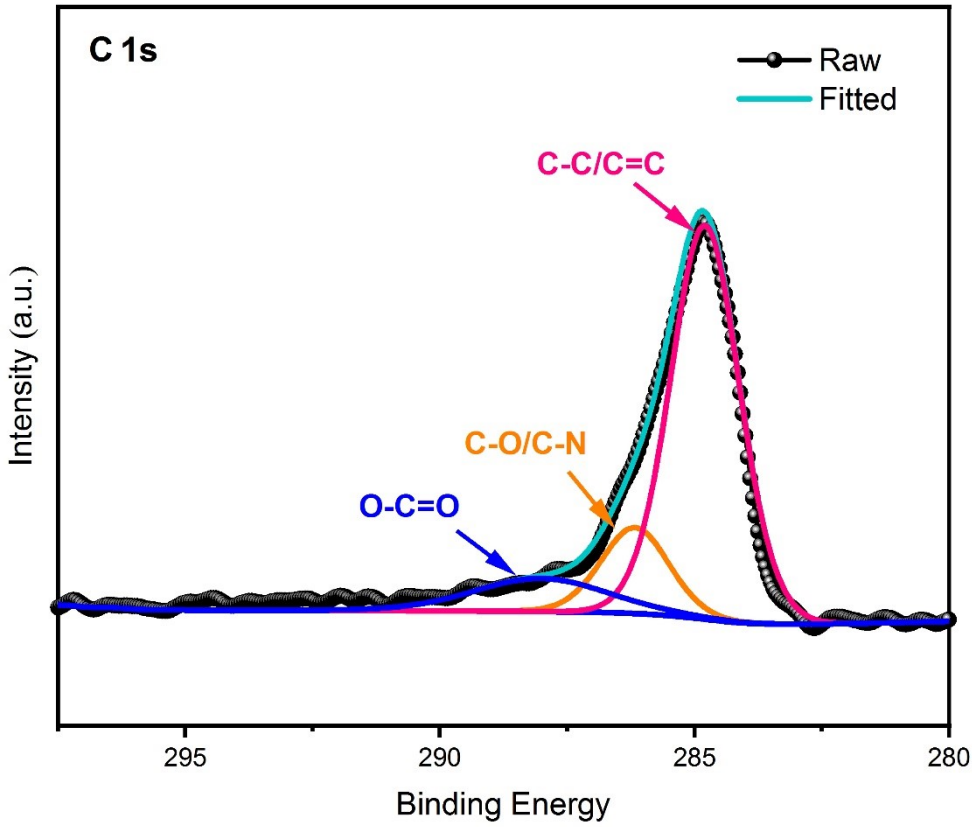

Figure S11 High-resolution XPS spectrum of C 1s of CoS_2/NC@1T MoS_2.

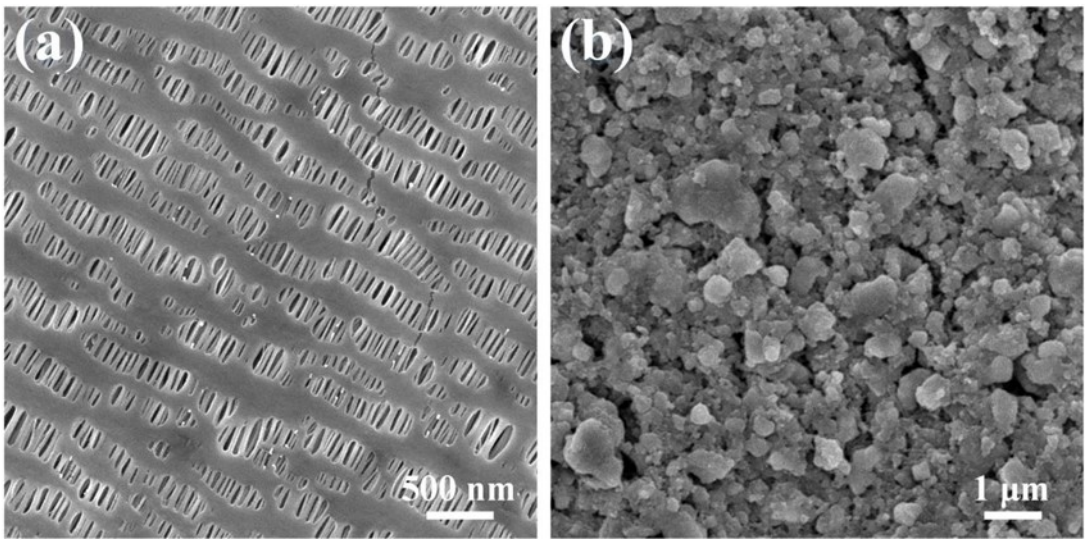

Figure S12 FESEM images of surfaces of (a) pure PP and (b) CoS_2/NC@1T MoS_2-PP separators before cycle.

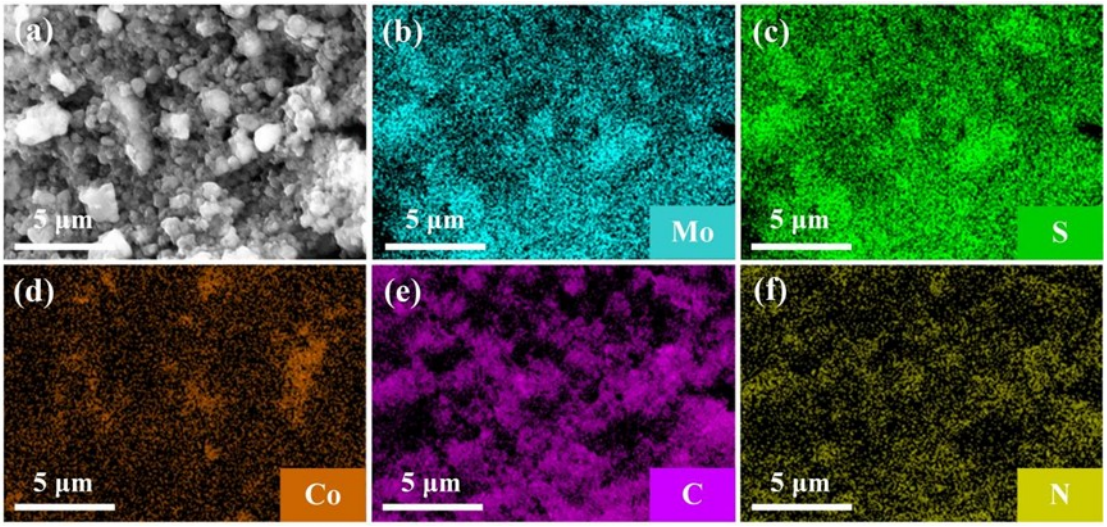

Figure S13 (a) Top STEM image of CoS_2/NC@1T MoS_2-PP separator, and (b-f) corresponding elemental mappings of Mo, S, Co, C, and N.

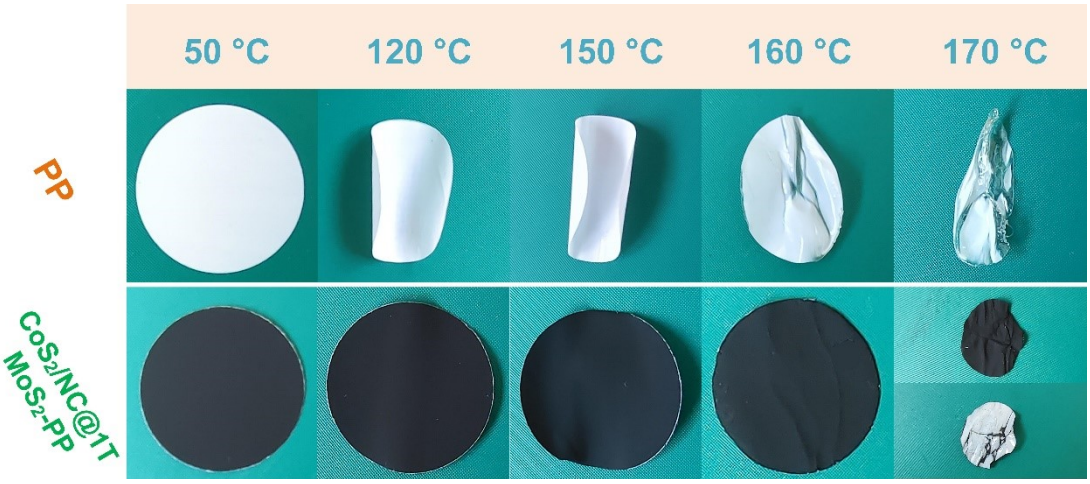

Figure S14 Photographs of PP and CoS_2/NC@1T MoS_2-PP separators after heat treatment.

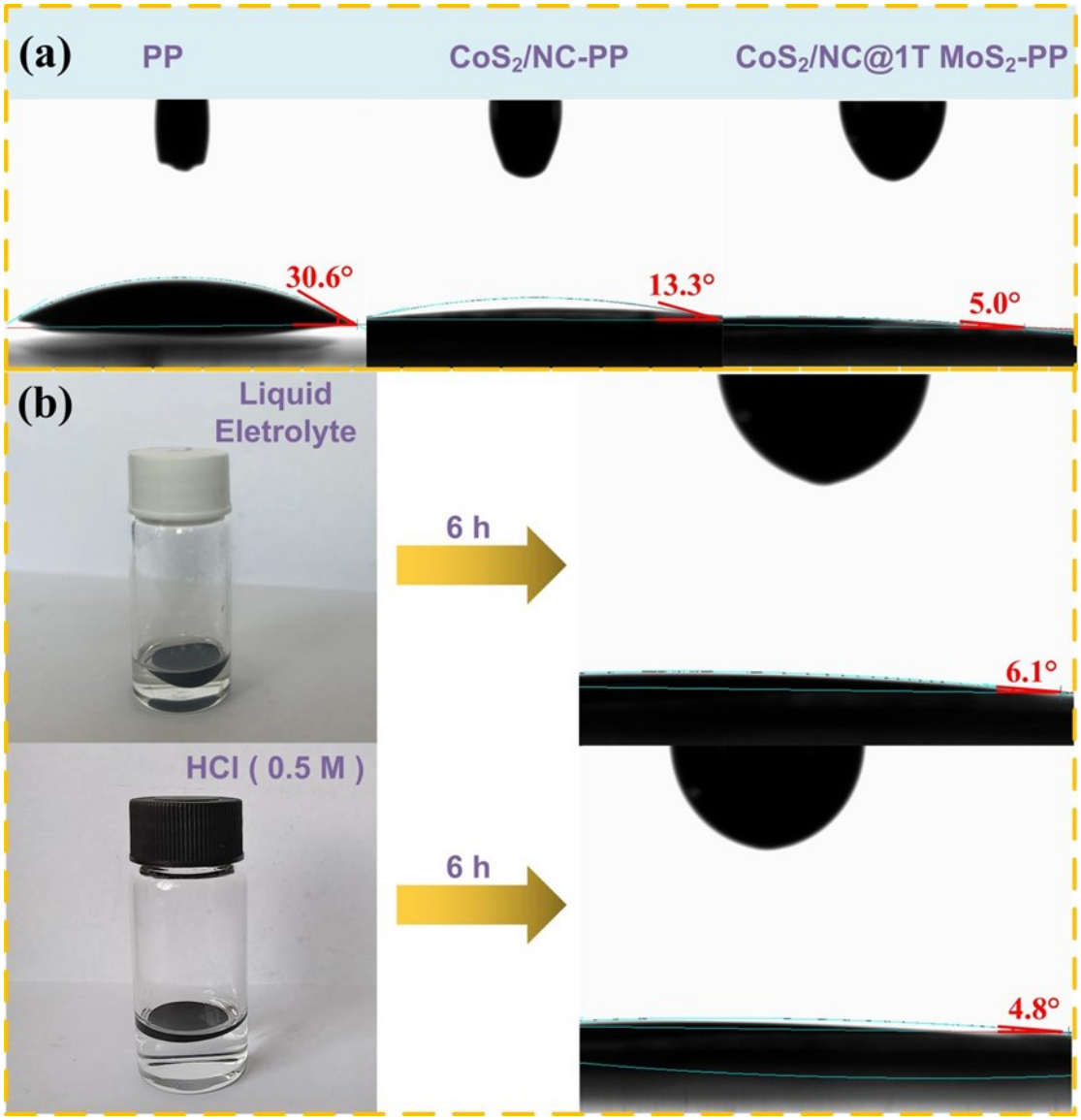

Figure S15 (a) Wettability of pure PP, CoS_2/NC-PP, and CoS_2/NC@1T MoS_2-PP separators. (b) Chemical stability of CoS_2/NC@1T MoS_2-PP separator.

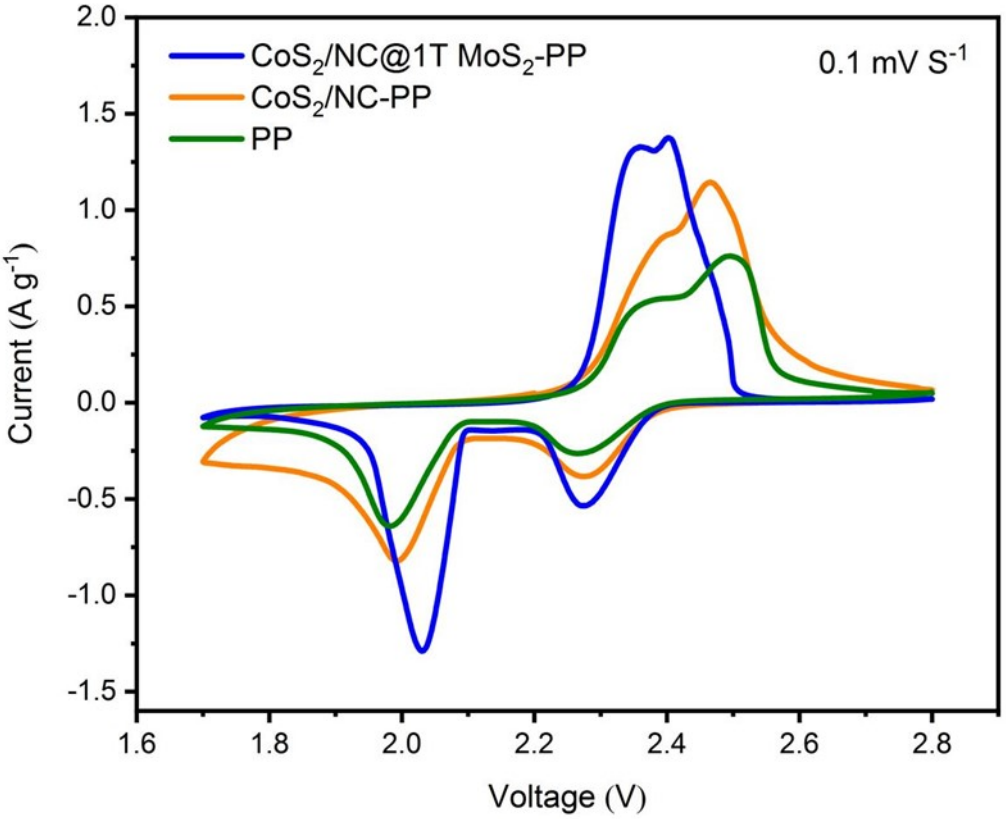

Figure S16 CV curves of lithium-sulfur batteries with CoS_2/NC@1T MoS_2-PP, CoS_2/NC-PP, and pure PP separators at a scan rate of 0.1 mV S^{-1}.

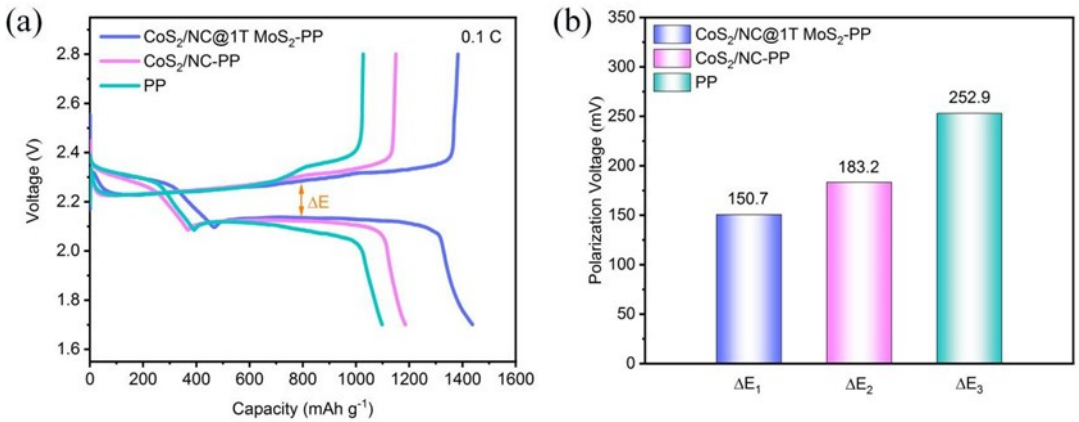

Figure S17 (a) Initial charge/discharge curves and (b) corresponding polarization voltage bar graphs of lithium-sulfur batteries with CoS_2/NC@1T MoS_2-PP, CoS_2/NC-PP, and pure PP separators at 0.1 C.

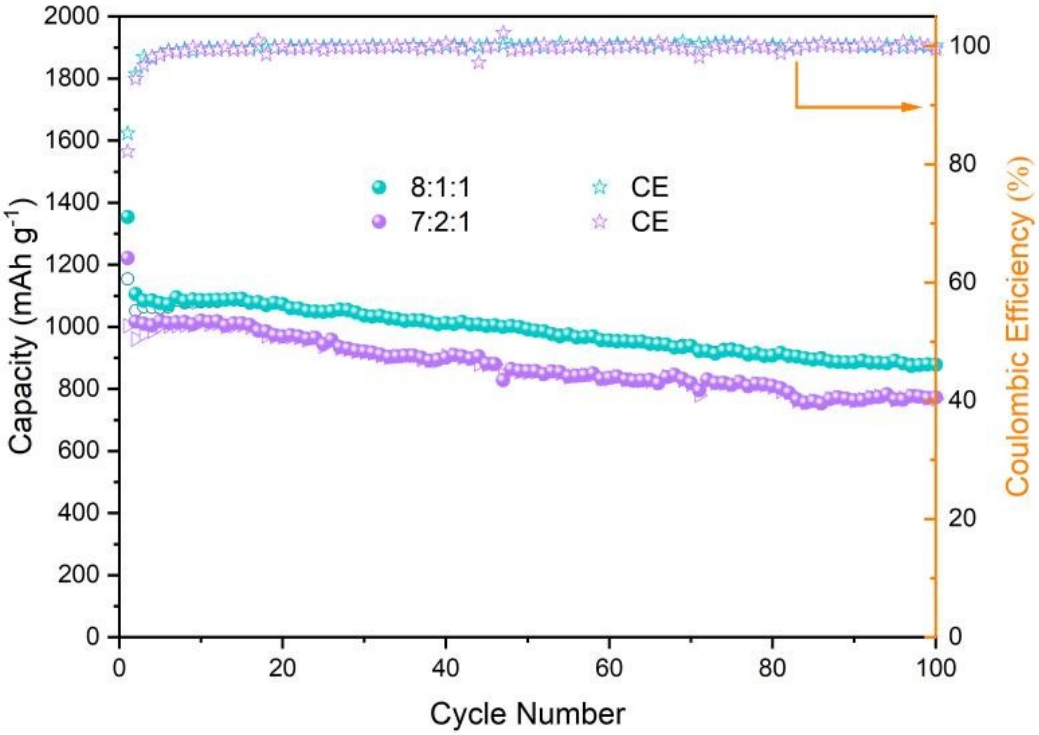

Figure S18 Cycle performance and coulombic efficiency of lithium-sulfur batteries with CoS_2/NC@1T MoS_2-PP separator for 100 cycles at a current density of 0.2 C at different positive slurry ratios.

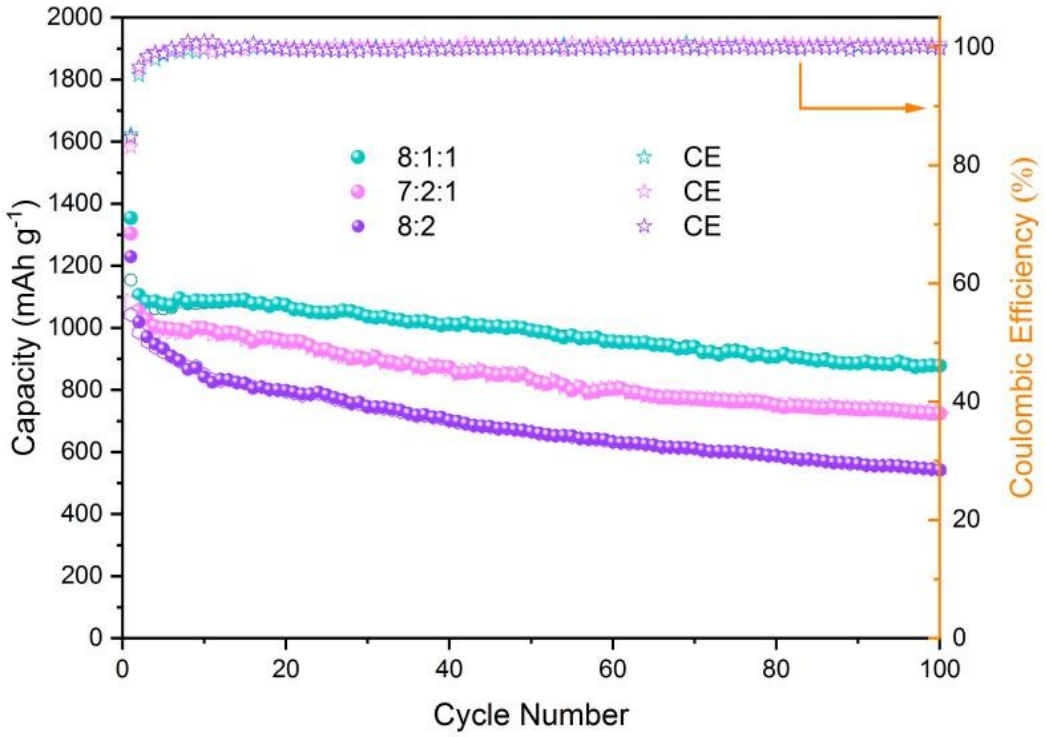

Figure S19 Cycle performance and coulombic efficiency of lithium-sulfur batteries with CoS_2/NC@1T MoS_2-PP separator for 100 cycles at a current density of 0.2 C at different separator slurry ratios (8:2, no acetylene black).

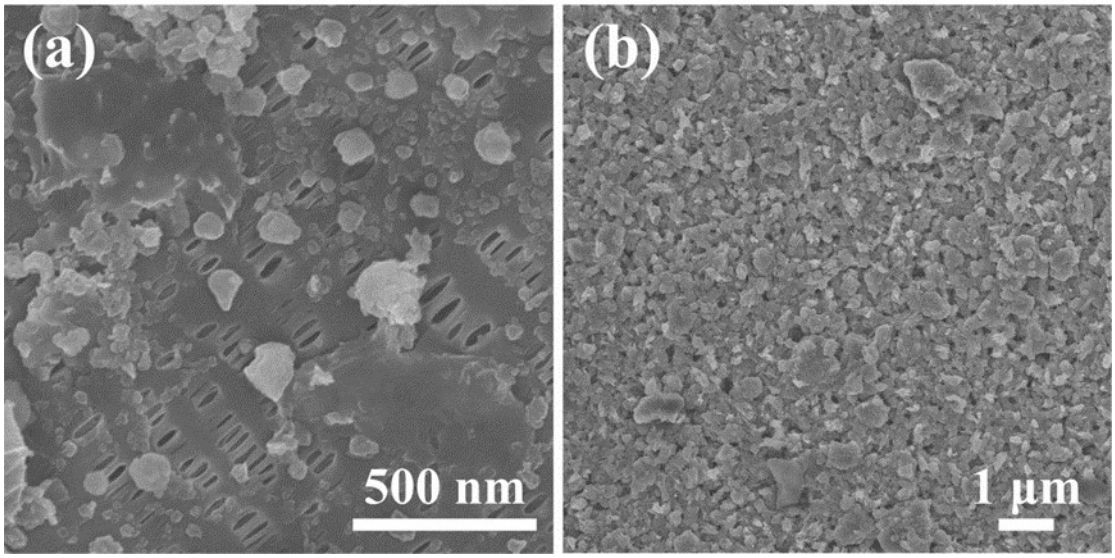

Figure S20 SEM images of surfaces of (a) pure PP and (b) CoS_2/NC@1T MoS_2-PP separators after cycles.

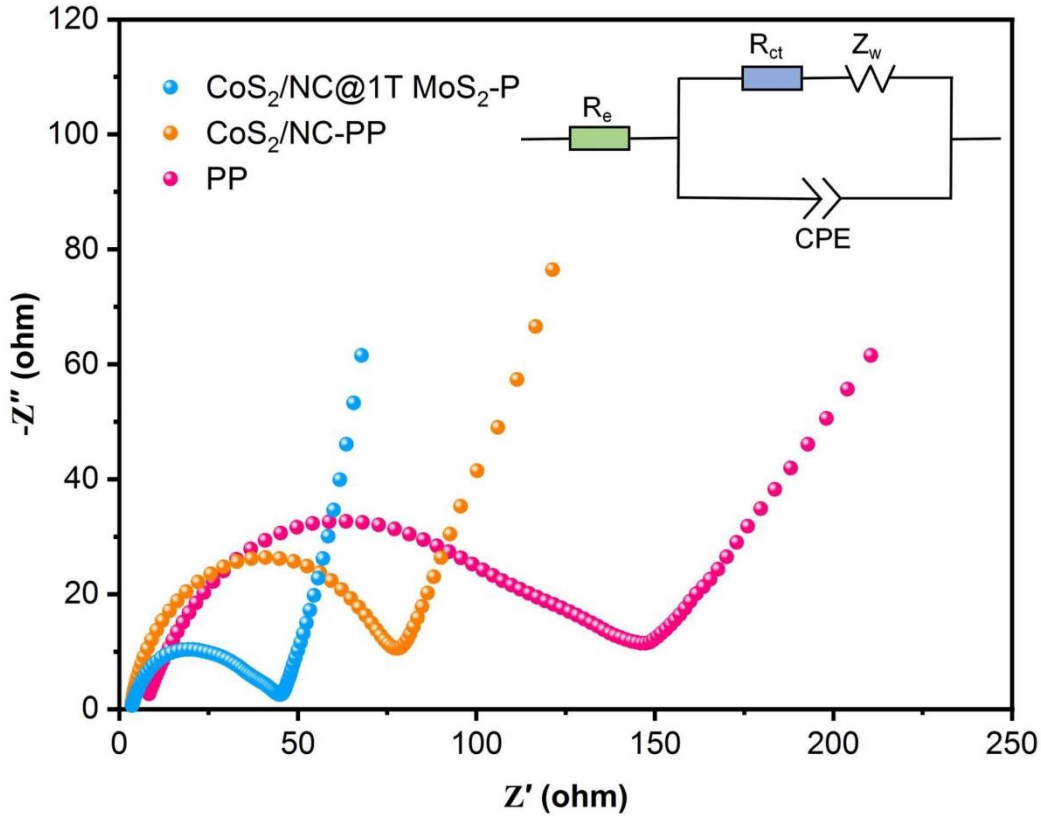

Figure S21 AC impedance spectra of lithium-sulfur batteries with CoS_2/NC@1T MoS_2-PP, CoS_2/NC-PP, and pure PP separators before cycle (inset: equivalent circuit).

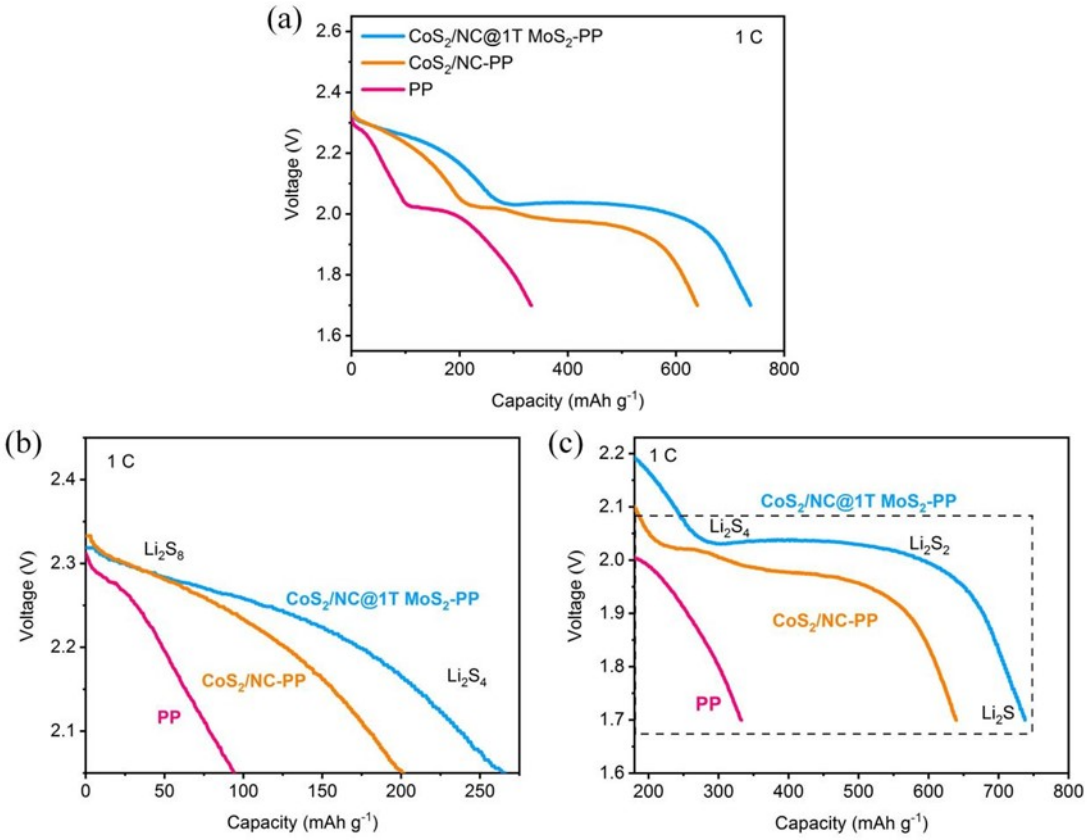

Figure S22 (a) Discharge curves of lithium-sulfur batteries with CoS_2/NC@1T MoS_2-PP, CoS_2/NC-PP, and pure PP separators at a current density of 1 C, and comparison of discharge curves at (b) high voltage and (c) low voltage at a current density of 1 C.

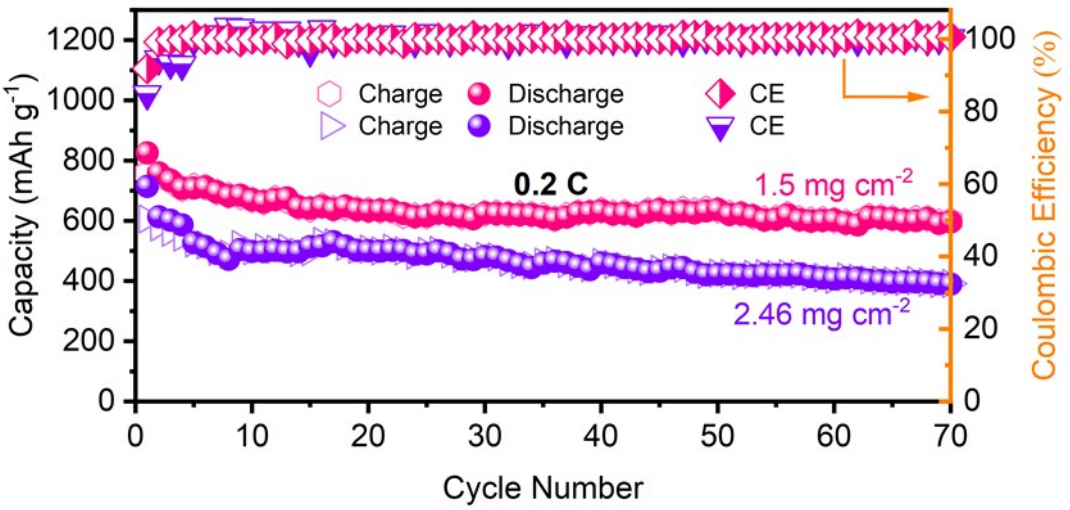

Figure S23 Cycle performance of LSBs with different high sulfur loadings at 0.2 C.

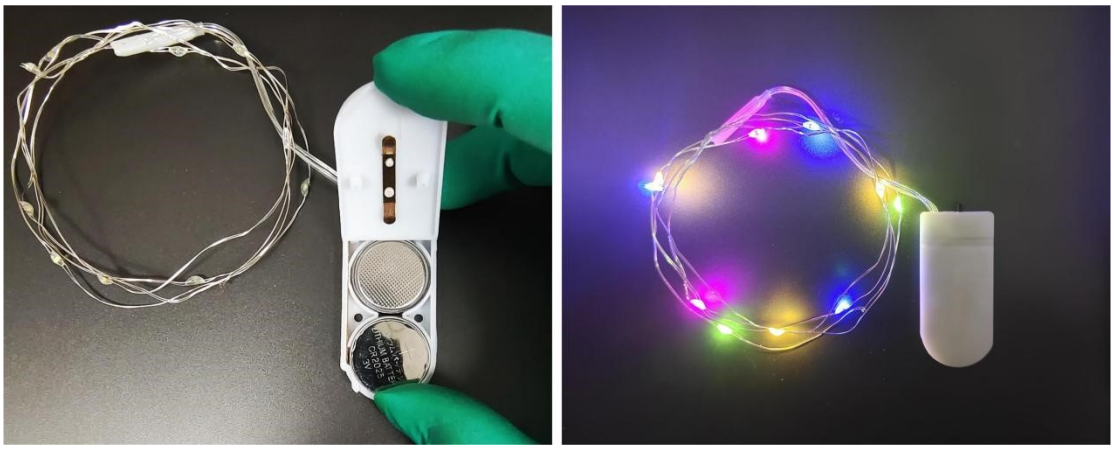

Figure S24 Digital photos of a light-emitting diode (LED) four-color lamp string lit up by CR2025-type lithium-sulfur batteries with CoS_2/NC@1T MoS_2-PP separator.

Table S1 Comparison of electrochemical properties of LSBs with CoS_2/NC@1T MoS_2-PP separator with previously reported LSBs.

Sample	Current density	Cycle number	Discharge capacity (mAh g^{-1})	Capacity decay rate per cycle (%)	Ref.
CC/VN/Co@NCNTs	0.1 C	100	864.1	0.35	S1
N-MIMEC	0.1 C	100	971.3	0.253	S2
CoSe@NC	0.1 C	100	804.7	0.39	S3
MnO_2@SnO_2	0.1 C	100	806	0.39	S4
3D P-MoS_2	0.5 C	300	629.4	0.144	S5
TiO_2	0.5 C	400	612	0.104	S6
CP@NCNT@CoS_3	0.83 C	400	680	0.119	S7
CoS_2@NGCNs	1 C	300	519.4	0.075	S8
CoS_2/HPGC	1 C	500	519	0.07	S9
Co-NC@N-HCS	1 C	450	399.7	0.13	S10
CoS_2/ACCF	1 C	500	580	0.082	S11
FSC/MoS_2/CNTs	1 C	500	615.3	0.059	S12
CoS_2/NC@1T MoS_2	**0.1 C** **1 C**	**100** **500**	**972** **616**	**0.316** **0.07**	**This work**

Notes and references

S1 D. P. Cai, Y. X. Zhuang, B. Fei, C. Q. Zhang, Y. G. Wang, Q. D. Chen, H. B. Zhan, Self-supported VN arrays coupled with N-doped carbon nanotubes embedded with Co nanoparticles as a multifunctional sulfur host for lithium-sulfur batteries, *Chem. Eng. J.*, 2022, **430**, 132931.

S2 H. Y. Shao, F. Ai, W. K. Wang, H. Zhang, A. B. Wang, F. Wang, Y. Q. Huang,

Crab shell-derived nitrogen-doped micro-/mesoporous carbon as an effective separator coating for high energy lithium-sulfur batteries, *J. Mater. Chem. A*, 2017, **5**, 19892-19900.

S3 X. L. Jiang, S. Zhang, B. B. Zou, G. C. Li, S. L. Yang, Y. Zhao, J. B. Lian, H. M. Li, H.B. Ji, Electrospun CoSe@NC nanofiber membrane as an effective polysulfides adsorption-catalysis interlayer for Li-S batteries, *Chem. Eng. J.*, 2022, **430**, 131911.

S4 P. Zhou, T. L. Han, C. P. Gu, J. J. Li, Z. H. Shen, H. G. Zhang, J. J. Niu, J. H. Liu, J.Y. Liu, A novel wheel-confined composite as cathode in Li-S batteries with high capacity retention, *J. Alloy Compd.*, 2019, **776**, 504-510.

S5 F. R. Liu, N. Wang, C. S. Shi, J. W. Sha, L. Y. Ma, E. Z. Liu, N. Q. Zhao, Phosphorus doping of 3D structural MoS_2 to promote catalytic activity for lithium-sulfur batteries, *Chem. Eng. J.*, 2022, **430**, 133923.

S6 Y. Yu, M. Yan, W. D. Dong, L. Wu, Y. W. Tian, Z. Deng, L. H. Chen, T. Hasan, Y. Li, B. L. Su, Optimizing inner voids in yolk-shell TiO_2 nanostructure for high-performance and ultralong-life lithium-sulfur batteries, *Chem. Eng. J.*, 2021, **417**, 129241.

S7 X. F. Yang, X. J. Gao, Q. Sun, S. P. Jand, Y. Yu, Y. Zhao, X. Li, K. Adair, L. Y. Kuo, J. Rohrer, J. N. Liang, X. T. Lin, M. N. Banis, Y. F. Hu, H. Z. Zhang, X. F. Li, R. Y. Li, H. M. Zhang, P. Kaghazchi, T. K. Sham, X. L. Sun, Promoting the transformation of Li_2S_2 to Li_2S: significantly increasing utilization of active materials for high-sulfur-loading Li-S batteries, *Adv. Mater.*, 2019, **31**, 1901220.

S8 S. D. Seo, D. Park, S. Park, D. W. Kim, “Brain-coral-like” mesoporous hollow CoS_2@N-doped graphitic carbon nanoshells as efficient sulfur reservoirs for lithium-sulfur batteries, *Adv. Funct. Mater.*, 2019, **29**, 1903712.

S9 Q. Q. Hu, J. Q. Lu, C. Yang, C. C. Zhang, J. L. Hu, S. Y. Chang, H. Y. Dong, C. Y. Wu, Y. Hong, L. Z. Zhang, Promoting reversible redox kinetics by separator architectures based on CoS_2/HPGC interlayer as efficient polysulfide-trapping shield for Li-S batteries, *Small*, 2020, **16**, 2002046.

S10 X. X. Sun, S. K. Liu, W. W. Sun, Y. J. Li, D. Q. Wang, Q. P. Guo, X. B. Hong, J. Xu, C. M. Zheng, Nano-confined synthesis of multi yolk-shell Co-NC@N-HCSs hybrid as sulfur host for high performance lithium-sulfur batteries, *Electrochim. Acta*, 2021, **398**, 139302.

S11 H. Yoon, D. Park, H. J. Song, S. Park, D. W. Kim, Vertically aligned sulfiphilic cobalt disulfide nanosheets supported on a free-standing carbon nanofiber interlayer for high-performance lithium-sulfur batteries, *ACS Sustain. Chem. Eng.*, 2021, **9**, 8487-8496.

S12 J. Ren, Y. B. Zhou, L. Xia, Q. J. Zheng, J. Liao, E. Y. Long, F. Y. Xie, C. G. Xu, D. M. Lin, Rational design of a multidimensional N-doped porous carbon/MoS_2/CNT nano-architecture hybrid for high performance lithium-sulfur batteries, *J. Mater. Chem. A*, 2018, **6**, 13835-13847.